terrain. Clementine bistatic radar data taken from other, intermittently sunlit areas with similar geometry, and subjected to the same data reduction process, show no evidence of such an enhancement. This leads to the conclusion that the scattering mechanism responsible for the orbit 234 enhancement is associated with the permanently shadowed terrain, which is suggestive of a muted CBOE originating from small patches of ice (and/or other frozen volatiles) covered and mixed with rocky material.

REFERENCES AND NOTES

1. K. Watson, B. C. Murray, H. Brown, *J. Geophys. Res.* **66**, 3033 (1961).
2. J. R. Arnold, *ibid.* **84**, 5659 (1979).
3. D. A. Paige, S. E. Wood, A. R. Vasavada, *Science* **258**, 643 (1992).
4. A. P. Ingersoll, T. Svitek, B. C. Murray, *Icarus* **100**, 40 (1992).
5. J. R. Salvail and F. Fanale, *ibid.* **111**, 441 (1994).
6. S. J. Ostro and E. M. Shoemaker, *ibid* **85**, 335 (1990).
7. K. J. Peters, *Phys. Rev.* **46**, 801 (1992).
8. S. Etemad *et al.*, *Phys. Rev. Lett.* **59**, 1420, (1987).
9. M. I. Mishchenko, *Astrophys. Space Sci.* **194**, 327 (1992).
10. E. E. Gorodnichev, S. L. Dudarev, D. B. Rogozkin, *Phys. Lett. A* **144**, 48 (1990).
11. M. I. Mishchenko, *J. Opt. Soc. Am.* **A 9**, 978 (1992).
12. ——, *Earth Moon Planets* **58**, 127 (1992).
13. B. Hapke, *Icarus* **88**, 407 (1990).
14. —— and D. Blewitt, *Nature* **352**, 46 (1991).
15. D. B. Campbell *et al.*, *Icarus* **34**, 254 (1978).
16. R. M. Goldstein and R. R. Green, *Science* **207**, 179 (1980).
17. S. Ostro, in *Satellites of Jupiter*, D. Morrison, Ed. (Univ. of Arizona Press, Tucson, 1982).
18. D.O. Muhleman, B. J. Butler, A. W. Grossman, M. A. Slade, *Science* **253**, 1508 (1991).
19. E. J. Rignot, S. J. Ostro, J. J. van Zyl, K. C. Jezek, *ibid.* **261**, 1710 (1993).
20. E. J. Rignot, *J. Geophys. Res.* **100**, 9389 (1995).
21. J. K. Harmon *et.al.*, *Nature* **369**, 213 (1994).
22. M. A. Slade, B. J. Butler, D. O. Muhleman, *Science* **258**, 635 (1992).
23. B. J. Butler, D. O. Muhleman, M. A. Slade, *J. Geophys. Res.* **98**, 15003 (1993).
24. V. Eschleman, *Science* **234**, 587 (1986).
25. N. J. S. Stacy, thesis, Cornell University (1993).
26. S. Nozette *et al.*, *Science* **266**, 1835 (1994).
27. E. M. Shoemaker, M. S. Robinson, E. M. Eliason, *ibid.*, p. 1851.
28. P. D. Spudis *et al.*, *Lunar Planet. Sci.* **XXVI**, 1339 (1995).
29. P. D. Spudis *et al.*, *Science* **266**, 1848 (1994)
30. P. D. Spudis, in *The Geology of Multi-ring Impact Basins* (Cambridge Univ. Press, Cambridge, 1993).
31. M. T. Zuber *et al.*, *Science* **266**, 1839 (1994).
32. R. A. Simpson, *IEEE Trans.* **GRS-31**, 465 (1993).
33. Analysis was conducted using fast Fourier transform (FFT) techniques. The target area is isolated by Doppler shift, which relates bands of constant frequency to a set of lunar ground locations (the $\beta = 0$ track). The ground points were close enough in distance to include all of the bands of constant frequency in the selected area. Repeat responses were filtered out. The analyses to extract radar scattering information from local regions on the surface were performed by sorting the Doppler data according to the parameter of interest. Typical frequency domain transform parameters used were 1 to 4 seconds of noncoherent averaging, 4096 to 16,384 points per FFT, a von Hann time data window without zero-padding, and magnitude-only (power) data stored in double-precision output.
34. J. V. Evans and T. Hagfors, Eds., *Radar Astronomy* (McGraw-Hill, New York, 1968).
35. The effective system noise temperature baseline was estimated by comparing measured noise from the zenith (20 K), moon center (235 K), and lunar poles (90 K). Measurements of ambient temperature microwave resistors added further corroborating measurements to the set of calibration data. The noise baseline, when considered against the recorded attenuator values, was used to calibrate the amplitude of the data files into units of signal-to-noise ratio (SNR). Calibration to flatten the frequency response variation arising from receiver filters was performed using noise-only segments of data. The calibrations included: linear gain change, nonlinear gain change, recording channel frequency response, system noise temperature changes, erroneous data bridge-over, transmitter frequency variation, transmitter power variation, and antenna pointing. A small amount of corrupted data is inevitably recorded. The short periods of corrupted data were flagged and suppressed during subsequent analyses. Spacecraft attitude files were corrected for known time-base and pointing systematic errors. One-way light-time propagation delay effects were included. Systematic errors that simultaneously affect the absolute baseline or bias measurement of each polarization channel were estimated to be less than ± 2 dB. Systematic errors in the ratio measurements are estimated at ± 0.25 dB. The systematic errors common to both channels are suppressed when considering the ratio. Thermal noise variation is negligible because several hundred to several thousand frequency bins were averaged together, each having a thermal SNR greater than 10. Target speckle variation is believed to be the dominant stochastic error source. The mean value and error bars given in Fig. 3 are derived by reducing the data set standard deviation by the square root of the number of noncoherently averaged samples represented by each point on the plot. The use of noncoherently averaged FFTs and numerous frequency bins reduced this variation to about ± 0.1-0.2 dB standard deviation. Median filtering was used. Due to the time sampling, regional averaging, and spacecraft system characteristics the resolution in β is $\pm 0.2°$. Due to Doppler bin migration (± 1 bin), phase noise of the spacecraft oscillator (± 2 bins), and FFT windowing effects (± 2 bins), the Doppler band regions have an estimated rms resolution uncertainty of about ± 25 km at $-80°$ latitude, for the 16,384 point FFT data files.
36. L. Tsang, J. A. Kong, R. T. Shin, *Theory of Microwave Remote Sensing* (Wiley-Interscience, New York, 1985).
37. A standard analysis of variance (ANOVA) for unbalanced design was performed on the data from each orbit. ANOVA tests the null hypothesis that the means are the same and only appear different in measurement because of random fluctuations in the data. This analysis tests the statistical significance of the differences among the means. The data represented target return bins corresponding to angles of incidence greater than 82°.

38. The authors thank the NASA/JPL and Deep Space Network individuals who supported and helped carry out these observations, in particular S. Asmar; the Clementine lunar operations team led by T. Sorensen, assisted by R. Campion and T. Tran; P. Rustan of the U.S. Air Force, the Clementine 1 program manager, D. Duston of BMDO, and L. Wood of LLNL; and R. Simpson and G. Pettengill for review and insight. Funding for this work was provided by the Department of Defense, including the Ballistic Missile Defense Organization, the Naval Research Laboratory, the U.S. Air Force Phillips Laboratory Space Experiments Directorate, the Department of Energy, Lawrence Livermore National Laboratory, and NASA. This paper is Lunar and Planetary Institute contribution 899.

3 June 1996; accepted 22 October 1996

Stabilizing Lead-Salt Diode Lasers: Understanding and Controlling Chaotic Frequency Emission

Gordon Chin, Larry R. Senesac, William E. Blass, John J. Hillman

Lead-salt tunable diode lasers (TDLs) are the only devices currently available that can generate tunable monochromatic radiation at arbitrary wavelengths between 3 and 30 micrometers and are particularly useful for high-resolution spectroscopy over a wide range of spectral regimes. Detailed observations of TDLs show that the observed instrumental linewidth is actually a temporal average of many narrow (less than 0.5 megahertz) emission "modes." The time scale characteristic of these "modes," which appear to be of relatively constant intensity, is of the order of a microsecond. The laser's behavior is highly suggestive of a chaotic process, that is, seemingly random excursions of a dynamic variable (frequency) within a bounded range. This report shows experimentally that TDL emissions are indeed chaotic. Furthermore, in a simple and robust fashion, this chaotic behavior has been successfully controlled with the use of recent techniques that take advantage of chaos to produce a narrow band laser output.

Chaotic behavior is an intrinsic property of a nonlinear system. Mechanical systems, communication and electronic systems, biological systems, the solar system, optical and laser systems, and many other nonlinear systems often exhibit chaotic behavior. Chaos is also often called deterministic random motion. The motion is deterministic because its trajectory can be calculated for all times given the starting conditions, but it is also motion in which instabilities appear everywhere in the system's trajectory in phase

G. Chin and J. J. Hillman, NASA Goddard Space Flight Center, Laboratory for Extraterrestrial Physics, Greenbelt, MD 20771, USA.
L. R. Senesac and W. E. Blass, Department of Physics and Astronomy, University of Tennessee, Knoxville, TN 37996–1200, USA.

space, the coordinate system describing a system's position and velocity. These instabilities force the trajectories of nearby phase-space points to diverge. This divergence is manifested as a sensitivity to initial conditions, another characteristic of chaotic motion. However, the nonlinearities of the system fold the trajectories back into a confined region. In this manner, chaotic motion amplifies small differences, errors, or noise, that is, the instabilities stretch phase space, whereas the nonlinearities, or folding motion, keep the trajectories bounded. Bounded trajectories signal the presence of an attractor. Another indication of chaotic behavior is the existence of a "strange" attractor with its distinctive fractal character. It is this fractal characteristic that gives chaotic motion its random appearance.

More recently, investigations of nonlinear dynamics have moved from purely theoretical and computational studies to experiment. Some of these experiments show that chaotic behavior is a useful feature in itself and more importantly may be exploited to perform practical functions (*1*). Following theoretical studies that reveal methods that stabilize unstable orbits (*2*, *3*), a set of striking experiments ensued that demonstrated that chaos can be controlled in a surprisingly simple manner (*4*, *5*) and in as diverse a range of problems as cardiac arrhythmia (*6*), thermal convection loops (*5*), electronic circuitry (*7*), an optical system (*8*), and solid-state lasers (*9*).

The practical demonstration of chaos control led us to consider whether these techniques are applicable to tunable diode lasers (TDLs). Lead-salt TDLs are valuable tools that are used to measure the molecular parameters of atmospheric constituents important in planetary atmospheres (*10*). The advantages of TDLs are wide spectral coverage (3 to 30 μm), achieved by varying the salt composition of an epitaxially grown lead-salt crystal (such as $Pb_{1-x}Sn_xTe$ or $PbS_{1-x}Se_x$), and high spectral resolution ($\sim 10^{-4}$ cm^{-1}). The TDLs are operated below 100 K and are tuned by changing the temperature or injection current (which effectively causes a change in the temperature of the laser junction). The combination of wide spectral coverage, continuous tunability, high resolution, high output power, and ease of use makes TDLs ideal for the study of line positions, line strengths, and pressure broadening coefficients, especially of molecules with closely spaced spectral transitions.

Despite the extremely successful use of TDLs in laboratory spectroscopy, the full potential of the TDL has not been realized. Careful characterization of a TDL shows that the intrinsic linewidth of its emission is very narrow (<0.5 MHz or $\sim 10^{-5}$ cm^{-1}), a factor of 10 better than the instrumental resolution achieved in laboratory applications. The observed instrumental linewidth is actually a temporal average of many narrow frequency emissions or "modes" (*10*, *11*). These instantaneous modes, which are relatively constant in intensity, change on a time scale on the order of a microsecond. This behavior is a natural consequence of the intrinsically nonlinear operation of a laser junction, where many microscopic facets or lasing regions may exist. Minute changes in the junction—such as in temperature, dimension, or index of refraction—can quench one lasing mode while allowing another to reach threshold. The detailed dynamics of such a complicated system is probably not amenable to analytical description.

Fortunately, numerical methods exist that can identify the presence of chaotic behavior without requiring a detailed knowledge of the underlying dynamics. However, the challenge remains how to capture the trajectory of the TDL in which the dynamical variable, frequency, varies at a megahertz rate. This information is also critical in our goal to control the TDL's chaotic emission.

The solution is to construct a frequency-to-amplitude converter (F/A) with a fast response time. We use one of two approaches: either an absorption cell containing a gaseous molecular sample or a Fabry-Perot etalon is placed in the path of the TDL's beam. By adjusting the TDL to lase on the steep side of either the gas line or the Fabry-Perot fringe, changes in the TDL frequency are converted to changes in detected signal amplitude. The F/A we used was an absorption transition of ethylene (C_2H_4) near 1029 cm^{-1} (Fig. 1A). However, an etalon or any other gas line within the tuning range of the TDL can work just as well. The advantages of using a gas absorption line are minimal losses in photon flux compared with those for a high-finesse etalon and the ability to control the slope of the F/A conversion by varying the pressure in the absorption cell.

We looked for signatures of chaotic behavior with several numerical tools. We first examined the power spectrum (*12*). Periodic oscillations in the data would produce spikes in the power spectrum. The power spectrum from our data is very broad, indicating that the emissions are not purely periodic. The largest Lyapunov exponent—a measure of the rate at which trajectories initially close together in phase space diverge (*12*, *13*)—is 0.238 ± 0.022 for the filtered data in Fig. 1A, and the values ranged from 0.269 ± 0.013 to 0.314 ± 0.011 in other measurements. Positive Lyapunov exponents characterize chaotic data, whereas periodic data have negative values. There are two tests that measure the dimension of the chaotic attractor in phase space: the capacity (or Hausdorff) dimension (*12*) and the correlation dimension (*14*). Both measures yield a dimension of about 4 for the raw TDL data (and about

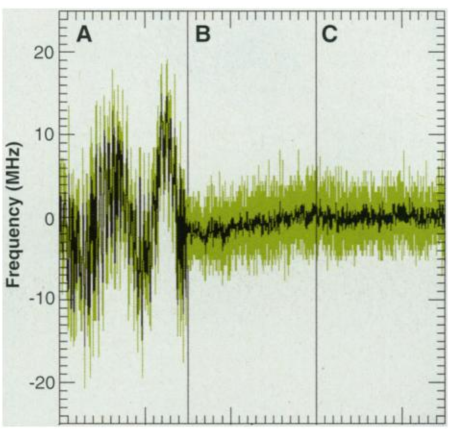

Fig. 1. The frequency variation of a lead-salt TDL operating near 1029 cm^{-1} using a line of ethylene as the F/A converter. Each panel has 30,000 points digitized with a 20-MHz 8-bit analog-to-digital converter. The colored points are the measured data. The black plot shows the results of applying a digit low-pass filter to the measurements. The frequency scale was calibrated with the use of methods similar to those used in (*10*, *11*). **(A)** Chaotic TDL emission without control. **(B)** TDL emission with the OPF electronics on. **(C)** Detector noise level when the laser beam is blocked. The difference between the filtered and unfiltered data is identical to the noise, showing that we succeeded in taking out only the detector noise. The interval of the measurements was 1.5 ms; the data in the three panels were not taken contiguously.

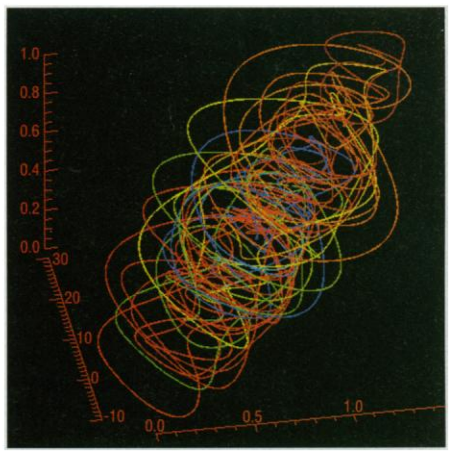

Fig. 2. A 3D time-delay phase plot of the TDL frequency trajectory from the measurements displayed in Fig. 1A. The trajectory shows intricate spiral structure embedded within spiral structure. An animated version of this figure reveals stretching and folding motions. The points are colored to show the time evolution of the trajectory from blue to red. The axes indicate frequency in megahertz.

1.268 ± 0.070 for the filtered data). We also performed a single-value decomposition (*15*) of our raw and filtered data, which resulted in only three significant eigenvalues and eigenvectors, again indicating that the TDL trajectory has a low degree of complexity.

A three-dimensional (3D) phase-space portrait (*16*) of the TDL filtered data using time-delay coordinates (Fig. 2) reveals a trajectory that is composed of strikingly complex embedded spirals. For stochastic data or random noise, such a plot shows no structure, and the trajectory randomly fills phase space. If the data are periodic, then the trajectory forms a closed orbit. An animated 3D phase portrait (*17*) shows the stretching and folding motions in the TDL frequency excursions. The TDL trajectory is confined, yet it never repeats—again a signature of chaos.

Because the TDL emission did appear chaotic, our next goal was to control this chaotic behavior. In 1990, Ott, Grebogi, and Yorke (OGY) (*2*) set the theoretical stage for chaos control based on the idea that the chaotic attractor of a system is made up of an infinite number of unstable orbits. The first step in the OGY method is to monitor one (or some) of the system variables and use the time-delay coordinate embedding technique (*16*) to construct the attractor for the system. From this attractor, they choose an orbit that yields the desired behavior and then locate the fixed points of that orbit. Finally, they apply a small time-dependent perturbation to an accessible system parameter to keep the fixed point in the path of the trajectory. The idea is to take advantage of the system's sensitive dependence on initial conditions and use minor perturbations to control chaos.

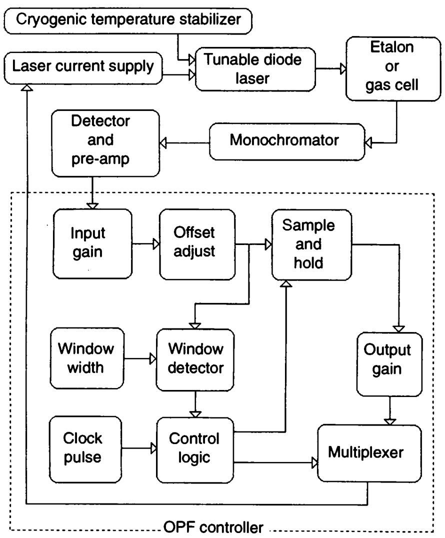

Fig. 3. Diagram of the setup for our TDL chaos control experiment.

In 1991, Hunt developed a modification of the OGY method called occasional proportional feedback (OPF) to find, stabilize, and switch between different orbits of a diode resonator (*7*). One advantage of the OPF method is that detailed knowledge of the dynamics is not necessary, nor is it required to know initially where the fixed points of the system lie. In fact, the OPF method can be used to allow the system to find stable orbits by itself. The basic method of OPF is to sample an accessible dynamical system variable, and if the value of the variable falls within a prescribed range or "window," a system parameter is modulated with an amplitude proportional to the difference between the value of the sampled variable and the center of the window. An explanation of why OPF works and an extension of this method using the duration of the feedback control as an additional control parameter that is effective for higher complexity systems is found in (*18*). The circuitry needed to implement the OPF method is extremely simple and easy to construct and has been successfully applied to a wide range of physical applications (*4*–*9*).

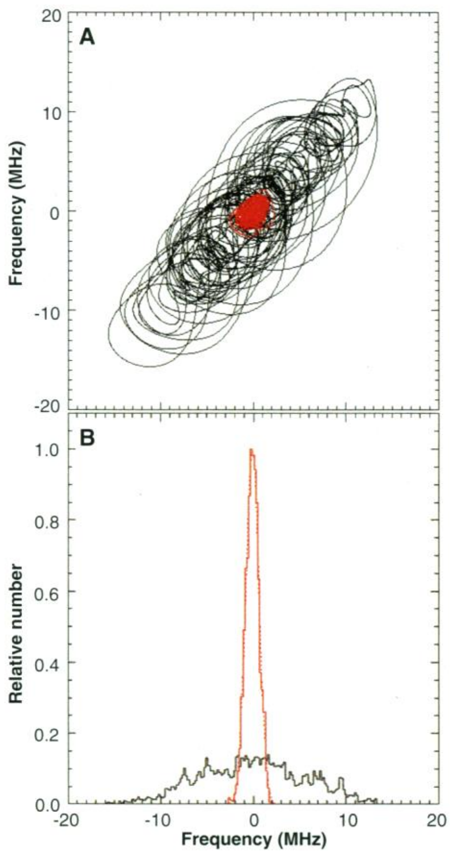

Fig. 4. (**A**) A 2D time-delay phase plot of the chaotic (black) TDL and OPF-controlled (red) trajectories from Fig. 1. (**B**) Histogram of TDL trajectories in (A) with 0.2-Mhz bins that shows the extent of the frequency variations. The red dash plot is a Gaussian fit to the OPF-controlled TDL data. The FWHM of the Gaussian, 1.68 MHz, is an upper limit to the stabilized TDL frequency. The chaotic TDL excursion is ~18 MHz.

For our problem, we monitor the frequency excursion, with the F/A method described above, and use the injection current of the TDL as the accessible system parameter (Fig. 3). The output frequency of a TDL is coarse-tuned by the operating temperature in a close-cycle refrigerator and fine-tuned by the injection current. The F/A output, from a detector preamplifier, enters the OPF electronics through a variable-gain input. An offset is added to the input signal to center it in a window. This signal is fed to a window detector and a sample-and-hold amplifier. The F/A signal is checked to determine if it lies within the adjustable width of the window. If so, the sampled signal is fed through a variable-gain output amplifier as a correction to the TDL control module, which adds it to the TDL injection current. The sampling rate and output correction signal are synchronized by an external clock, in our case running at 1 MHz.

Control of the TDL emission was established quickly in a simple and robust fashion as the gain of the correction signal was gradually increased: The chaotic TDL emission (Fig. 1A) can be contrasted to the stability acquired when OPF control is fully active (Fig. 1B). The controlled TDL emission is stable in both frequency and amplitude.

Our measurements are all dominated by detector noise (the colored plots in Fig. 1). Because it is primarily high frequency (Fig. 1C), we felt it appropriate to apply digital low-pass filtering to our data to improve our measurement accuracy. The amount of filtering was determined by the requirement to preserve the characteristic of the TDL chaotic emission without any distortion.

Several parameters determine how well the OPF method works. For example, TDL control is dependent on clock speed. For speeds slower than 600 kHz, OPF control fails; otherwise, the exact OPF clock speed is not critical: our experiments were all conducted at 1 MHz. This restraint is consistent with (*10*, *11*), and measurements here that show the time scale for TDL variations is ~1 μs. The sensitivity of the F/A conversion is another important factor. High sensitivity in the F/A conversion, that is, small values of $\Delta V/\Delta \nu$ (for voltage V and frequency ν), or the steepness of the line where the laser is tuned causes difficulty in control. The ethylene line we used has a 12 V/GHz slope (to convert from voltage variation to frequency, we used 81 MHz/V). The width of the OPF window, on the other hand, is not a sensitive parameter. Once stable TDL emission was established, OPF control was robust and continued indefinitely without further adjustment.

The slight drift in frequency in Fig. 1B is attributable to a small and slow 100-Hz ramp in the injection current from the TDL control module. This drift shows that OPF control can be maintained while varying the center frequency of the TDL. We achieved similar results with a fixed Fabry-Perot etalon as the F/A by tuning the TDL to one side of a low-finesse etalon fringe. We maintained OPF control while scanning the frequency over a range of ~80 MHz. This range is of practical importance as it demonstrates that OPF can be used with a TDL to scan across a molecular absorption feature and to perform spectroscopic measurements at higher frequency resolution than previously possible.

We can only give an upper limit to the frequency stability attained with the OPF method because the measurements are dominated by detector noise that can only be improved by signal processing (Fig. 1). Another factor is that our F/A process inseparably convolves amplitude and frequency variations. To calculate an upper limit, we project the trajectories in two dimensions (Fig. 4A). A histogram of the number of points in each 0.2-MHz bin of the controlled and uncontrolled emission is then made (Fig. 4B). From a Gaussian fit to the controlled distribution, we obtain a value for its full width at half maximum (FWHM), here being 1.68 MHz, which we can use as a strict upper limit.

An equal partitioning of the intensity and frequency variations in quadrature, a reasonable assumption, would reduce the frequency limit by $\sqrt{2}$, to 1.19 MHz. The FWHM of the uncontrolled TDL excursion, measured by hand, is ~18 MHz. Therefore, the OPF method improves the TDL frequency stability by at least a factor of 11 to 15. We can determine more accurately the frequency stability by heterodyning the TDL output with a stabilized 10-μm CO_2 laser.

The improved stability, in both the frequency and the amplitude of the OPF-controlled TDL, will enable new applications. We have mentioned higher resolution spectroscopy that scans a TDL. An OPF-controlled TDL can also be used as a local oscillator for heterodyne radiometers. The far-infrared (FIR) spectral regime is extremely important, and the recent development of wide-bandwidth hot-electron bolometer mixers makes the need for a suitable FIR local oscillator immediate. There are numerous candidates for future OPF control, such as an optically pumped submillimeter laser that emits from 30 μm to 1 mm and whose output varies in a seemingly random fashion because of nonlinear feedback between the pump and lasant gas.

REFERENCES AND NOTES

1. "Chaos in Communications," *Proc. SPIE 2038* (1993).
2. E. Ott, C. Grebogi, J. A. Yorke, *Phys. Rev. Lett.* **64**, 1196 (1990).
3. U. Dressler and G. Nitsche, *ibid.* **68**, 1 (1992); F. Romeiras, C. Grebogi, E. Ott, W. P. Dayawansa, *Physica D* **58**, 165 (1992); H. Wang and E. H. Abed, *Proceedings of IFAC Nonlinear Control Systems Symposium*, Bordeaux (1992).
4. W. L. Ditto, S. N. Rauseo, M. L. Spano, *Phys. Rev. Lett.* **65**, 3211 (1990).
5. J. Singer, Y.-Z. Wang, H. H. Bau, *ibid.* **66**, 1123 (1991).
6. A. Garfinkel, M. L. Spano, W. L. Ditto, J. N. Weiss, *Science* **257**, 1230 (1992).
7. E. R. Hunt, *Phys. Rev. Lett.* **67**, 1953 (1991).
8. T. Takizawa, Y. Liu, J. Ohtsubo, *IEEE J. Quantum Electron.* **30**, 334 (1994).
9. R. Roy, T. W. Murphy Jr., T. D. Maier, Z. Gills, E. R. Hunt, *Phys. Rev. Lett.* **68**, 1259 (1992); Z. Gills, C. Iwata, R. Roy, I. B. Schwartz, I. Triandaf, *ibid.* **69**, 3169 (1992).
10. D. E. Jennings, *J. Quant. Spectrosc. Radiat. Transfer* **40**, 221 (1988).
11. ———, *Appl. Opt.* **23**, 1299 (1984).
12. J. P. Eckmann and D. Ruelle, *Rev. Mod. Phys.* **57**, 617 (1985).
13. J. P. Eckmann, S. O. Kamphorst, D. Ruelle, S. Ciliberto, *Phys. Rev. A* **34**, 4971 (1986).
14. M. Ding, C. Grebogi, E. Ott, T. Sauer, J. A. Yorke, *Phys. Rev. Lett.* **70**, 3872 (1993).
15. D. S. Broomhead and G. P. King, *Physica D* **20**, 217 (1986).
16. N. H. Packard, J. P. Crutchfield, J. D. Farmer, R. S. Shaw, *Phys. Rev. Lett.* **45**, 712 (1980).
17. An animated phase portrait of one of our data sets can be viewed on our World Wide Web site at http://aurora.phys.utk.edu/~senesac/
18. T. W. Carr and I. B. Schwartz, *Phys. Rev. E* **51**, 5109 (1995); *Physica D*, in press.

19. We thank J. Lobell for designing the OPF electronics and G. Miller for putting it together [they are in Code 692 of the Goddard Space Flight Center (GSFC)]. M. Sirota and D. Reuter (Code 693) loaned us the diode laser for this experiment. This research was conducted under NASA cooperative agreement NCC 5-88 with the University of Tennessee under the support of the GSFC Director's Discretionary Fund.

29 July 1996; accepted 23 September 1996

Solar Wind Magnetic Field Bending of Jovian Dust Trajectories

H. A. Zook,* E. Grün, M. Baguhl, D. P. Hamilton, G. Linkert, J.-C. Liou, R. Forsyth, J. L. Phillips

From September 1991 to October 1992, the cosmic dust detector on the Ulysses spacecraft recorded 11 short bursts, or streams, of dust. These dust grains emanated from the jovian system, and their trajectories were strongly affected by solar wind magnetic field forces. Analyses of the on-board measurements of these fields, and of stream approach directions, show that stream-associated dust grain masses are of the order of 10^{-18} gram and dust grain velocities exceed 200 kilometers per second. These masses and velocities are, respectively, about 10^3 times less massive and 5 to 10 times faster than earlier reported.

While the Ulysses spacecraft was in the neighborhood of Jupiter, the on-board cosmic dust detector (CDD) detected 11 intense, and unexpected, streams of dust (*1–3*). The first stream occurred 2359 Jupiter radii (R_J, where 1 R_J = 71,398 km) from Jupiter, and 137 days before Ulysses' closest approach to Jupiter (JCA) on 8 February 1992. The last stream occurred at a distance of 4205 R_J, or about 2 astronomical units (AU), from Jupiter and 254 days after JCA. The dust grains in these streams are believed to have come from the jovian system (*2*) for two reasons: (i) the most intense stream, of 327 impacts onto the CDD, occurred only 31 days after JCA, and 327 R_J from Jupiter; (ii) stream radiants tended to lie on, or near, the line of sight (LOS) direction to Jupiter from the CDD. Both phenomena are shown in Fig. 1, where dust stream impacts are characterized by being unusually concentrated in the measured spacecraft rotation angle, ϕ_m, and in time (*4*). Each stream appears to impact the CDD from a single direction unique to that stream. The variation in ϕ_m is largely due to the 140° field-of-view (fov) of the CDD as it rotates through a stream radiant, although a few degrees of variation in ϕ_m may be due to a true spread in arrival directions of the dust grains. Strong non-gravitational forces must be acting on the grains during their trajectories from Jupiter because, under gravitational forces alone, average stream radiants would lie within a degree or two of the LOS direction to Jupiter. This was only true for streams S5 and S6. Analysis of CDD data from the Galileo spacecraft, which recorded even more intense streams of jovian dust than Ulysses (*5*), suggested that Jupiter's moon, Io, is a likely source of the dust (*6*).

H. A. Zook and J.-C. Liou, SN3, NASA Johnson Space Center, Houston, TX 77058, USA.
E. Grün, M. Baguhl, G. Linkert, Max-Planck-Institut für Kernphysik, Postfach 103980, 69029 Heidelberg, Germany.
D. P. Hamilton, Department of Astronomy, University of Maryland, College Park, MD 20742–2421, USA.
R. Forsyth, The Blackett Laboratory, Imperial College, London SW7 2BZ, UK.
J. L. Phillips, Los Alamos National Laboratory, Los Alamos, NM 87545, USA.

*To whom correspondence should be addressed. E-mail: zook@snmail.jsc.nasa.gov